Sensors & Actuators: B. Chemical 358 (2022) 131503

Contents lists available at ScienceDirect

Sensors and Actuators: B. Chemical

journal homepage: www.elsevier.com/locate/snb

PrGO decorated TiO_2 nanoplates hybrid nanocomposite for augmented NO_2 gas detection with faster gas kinetics under UV light irradiation

Nimmala Harathi [a,1], Manoj Bollu [b,1], Kedhaeswara Sairam Pasupuleti [c], Zhandos Tauanov [d], Koteswara Rao Peta [e], Moon-Deock Kim [c], Maddaka Reddeppa [f], Argha Sarkar [g,*], Vempuluru Navakoteswara Rao [h,*]

[a] Department of Electronics & Instrumentation Engineering, Sree Vidyanikethan Engineering College, Andhra Pradesh 517102, India
[b] Department of Physics, Sri Venkateswara University, Tirupati 517502, India
[c] Department of Physics, Chungnam National University, 99 Daehak-ro, Yuseong-gu, Daejeon 34134, Republic of Korea
[d] Faculty of Chemistry and Chemical Technology al-Farabi Kazakh National University, 050040 Almaty, Kazakhstan
[e] Department of Electronic Science, University of Delhi South Campus, Benito Juarez Road, New Delhi 110021, India
[f] Department of Electrical Engineering and Computer Science, University of Michigan, 1301 Beal Avenue, Ann Arbor, MI 48109-2122, United States
[g] Electronics and Communication Engineering, Vishnu Institute of Technology, Bhimavaram, Andhra Pradesh, India-534202
[h] National nanofab center, Korea advanced institute of science, Daejeon 34141, Republic of Korea

ARTICLE INFO

Keywords:
TiO_2 nanoplates
P-Phenylenediamine
rGO
Hybrid nanocomposite
NO_2 gas sensor

ABSTRACT

Controlling the anatase TiO_2 based-rectangular nanoplates (NPs) with {001} faces have gained immense interest in gas sensors applications, since the rectangular NPs of {001} planes are highly reactive for the adsorption of oxygen species that led to significant improvement in gas sensing performance. In this work, we report on the room temperature (RT) NO_2 gas sensing performances of hybrid nanocomposites with the interpenetrated network using *p*-Phenylenediamine-reduced graphene oxide (PrGO) decorated TiO_2 NPs. The fabricated TiO_2 NPs/PrGO heterostructure sensor demonstrated the superior NO_2 response (~14.9% to 100 ppm of NO_2) compared to TiO_2/rGO and pristine TiO_2 nanoplates. On the other hand, the TiO_2 NPs/PrGO heterostructure device showed high sensitivity, repeatability and excellent selectivity with short response/recovery times towards NO_2 gas at RT. Further, the performances of the TiO_2NPs/PrGO gas sensor was accelerated by UV irradiation ($\lambda = 365$ nm), and the response was found as ~35.68% to 100 ppm of NO_2 at RT, which was ~2.35-fold times higher than the dark condition. The high gas sensing performance would be attributed to the electrical sensitization of PrGO and the ample interface between TiO_2 NPs and PrGO that stimulated the charge separation with faster charge transport characteristics. Our strategy and results shed new light to exploit diverse functionalized materials to the high response gas sensors at RT.

1. Introduction

In recent years, the development of the smart gas sensors has become increasingly important for various applications such as, environmental pollution, health monitoring and safety of organic life [1,2]. Among the various toxic pollutant gases, especially, nitrogen dioxide (NO_2) is one of the common poisonous and toxic pollutants in the atmosphere, which is continuously being emitted from industries, automobiles, and coal combustion exhaust and it is also well-known hazardous gas that causes acid rain, which is harmful to the ecosystems [2,3]. Further, the precise monitoring of the NO_2 gas concentration in the breathing gas is essential in the heart valve surgery and diagnosis of asthma disease and even some times a few ppm concentrations of NO_2 lead to causes death [4,5]. Hence, the demand for cost-effective, highly sensitive, and reversible NO_2 gas sensors operative at room temperature (RT) are crucially important for environmental, civil applications and human health [6–10].

Among the various metal oxide semiconductor-based nanostructure such as SnO_2, WO_3, and ZnO, TiO_2 has gained great research attention toward toxic gas detection owing to their unique advantages of a

* Corresponding authors.
E-mail addresses: argha15@gmail.com (A. Sarkar), navakotinano@nnfc.re.kr (V.N. Rao).
[1] These two authors contributed equally to this work.

https://doi.org/10.1016/j.snb.2022.131503
Received 3 December 2021; Received in revised form 27 January 2022; Accepted 27 January 2022
Available online 4 February 2022

suitable band gap ~3.1 eV, high chemical stability, eco-friendly nature, nontoxic, and cost effective [16–19]. Further, tuning of the morphology, size, shape, crystal facets and surface properties of these materials have shown significant influence on the gas sensing properties [11,18]. Moreover, the anatase phase of TiO_2 based nanostructure with (001) facets has been widely used in gas sensing applications due to its high surface reactivity, since the unsaturated coordinate atoms and dangling bonds on (001) crystal facets, which greatly promotes the abundant oxygen deficiency that enriches the surface adsorbed oxygen species, further helps to enhance gas sensing performances [20]. However, the long response/recovery times and low sensitivity at RT, which are the bottlenecks for the practical applicability of TiO_2 based gas sensors [17]. To overcome, these issues it is to be necessary that the incorporation or integration of TiO_2 with the hybrid nanocomposite materials like graphene compounds, polymers and metal nanoparticles, which have been vastly considered to be an efficient approach to improve the gas sensing fidelity [17,18,20]. Recently, two-dimensional reduced graphene oxide (rGO) possessing reactive surface functional groups, high surface to volume ratio good electrical conductivity, and rapid electron transport kinetics, which has widely been utilized in NO_2 gas sensors [13–15]. However, plenty of oxygen functional groups in graphene allows the compatibility with organic moieties like *p*-Phenylenediamine (PPD) that would significantly improve the specific surface area and the conductivity [20]. In addition, PPD has been vastly used in different fields like sensing, electroanalytical detection, and energy storage devices, etc. due to their amine-rich functional groups [21,22]. Moreover, the carbon-based nanomaterials permit the molecular hybridization with PPD, which can obviously improve the sensitivity of the material that makes it more active and quickly responds to target gas molecules with high response. Hence, it is to be expected that the out coming composite matrix of PPD-rGO (PrGO) with TiO_2 would effectively demonstrate high conductivity, large surface area and abundant functional groups among the hybrid nanocomposite [18,20]. Further, the face-to-face contact of {001} faceted TiO_2 nanoplates with PrGO nanocomposite can generate a vertical heterostructure through Ti-O-C bonding that enforces the swift migration of charge carriers and boosting up the reactivity towards NO_2 gas molecules.

Usually, the TiO_2-based hybrid nanocomposites require high working temperatures to boosting up the adsorption/desorption gas kinetics [18]. However, the high operating temperature needs additional power supply unit which increases the fabrication cost and sometimes led to cause the ignition while detecting the flammable gas analytes that propels the growth of thermally induced oxide grains over the sensing material, which further deteriorate the sensor stability and hinders the long-term drift [18,20]. In order to avoid these issues, Ultraviolet (UV) light photo-activation is the finest strategy to stimulate the adsorption/desorption reactions on the metal oxide surfaces [18]. Since, the UV light induces the generation of free charge carriers that further boost up the electrical conductivity and enhance the desorption rate of gas molecules from the -hybrid nanacomposite surface, resulting in a short recovery time, good reversibility and high response to the NO_2 gas at RT.

In the present study, we demonstrated the successful fabrication of hybrid nanocomposites of TiO_2 nanoplates with (001) facets and PrGO for the effective NO_2 gas detection at RT. The NO_2 gas sensing performances of the TiO_2NPs/PrGO hybrid nanocomposite was studied under UV light illumination, different temperature conditions and relative humidity conditions as well. The-as prepared hybrid sensor showed a significant gas sensing responses to the NO_2 gas at RT under UV light which was ascribed to the synergetic effect of the hybrid nanocomposite and the underlying gas sensing mechanism was explored using an energy band diagram.

2. Experimental section

All the chemical reagents including Titanium butoxide ($Ti(OBu)_4$), hydrofluoric acid (HF), Graphene oxide (GO), and *p*-Phenylenediamine (PPD) were purchased from, Sigma-Aldrich (South Korea).

2.1. TiO_2 NPs/PrGO nanocomposite synthesis

The synthesis of TiO_2 nanoplates were synthesized using hydrothermal process as per the reported literature [10,18]. In brief, a 25 mL of Ti $(OBu)_4$ and 3 mL of HF were mixed together in the 100 mL of Teflon reactor, then sealed and maintained at 180 °C for 24 h. After reaction temperature getting down to the RT, the resultant TiO_2 nanoplates (NPs) precipitates collected and washed with ethanol and deionized water for many times. Finally, the white color precipitates of TiO_2 NPs were obtained after drying at 80 °C for 10 h. The pristine TiO_2 NPs solution was prepared by dissolving the obtained TiO_2 NPs precipitates in the 10 mL of deionized water (DI water) and then sonicated for 20 mins at RT.

In order to prepare the reduced-GO (rGO), GO solution was applied on a quartz substrate and then dried at 800 °C under argon ambient. Further, the obtained rGO (10 mg) was dispersed in the DI water (15 mL) followed by an ultra-sonication for 1 h for better dispersion. Next, PPD (13 mg) was dispersed in 20 mL of DI water sonicated for 10 min. Thereafter, the optimized proportional ration (2:3) of rGO and PPD solution were mixed together and continuously stirred at 60 °C for 5 h to obtain the PrGO composite. Further the optimized TiO_2 NPs/PrGO hybrid nanocomposite was prepared by adding 5 mL of TiO_2 NPs and 2 mL of PrGO in small beaker then sonicated for 30 mins for the better interaction between nanocomposite.

2.2. Fabrication of TiO_2 NPs/PrGO resistive gas sensor device

The full details of the fabrication process of TiO_2 NPs/PrGO gas sensor was schematically displayed in Fig. 1(a-b). First, Si/SiO_2 substrates were cleaned properly using acetone, methanol, and isopropyl alcohol for 5 min each. Next, the substrates were rinsed in DI water, and dried by blowing N_2 gas respectively. Next, the interdigitated electrodes of gold (Au) with a thickness of 100 nm were deposited by using direct current sputtering. The optimized concentrations of TiO_2 NPs, TiO_2 NPs/rGO, and TiO_2 NPs/PrGO hybrid nanocomposites were drop-casted individually on Au IDT electrodes coated substrates followed by one-day in air-drying at RT. The schematic diagram of our dynamic mode gas sensing system as shown in Fig. 1(c). Here two gas cylinders filled with dry air and NO_2 gas. NO_2 gas contains 1000 ppm balanced with N_2 and flow rate was allowed at 300 sccm. One could note that carrier gas is flowing continuously thought the experiment. The relative target gas concentrations in the carrier gas flow can be estimated by using the following Eq. (1) [23]. Humidity in the test chamber was internationally created by passing the dry through water bubbler jar as displayed in the Fig. 1(c). The humidity and the temperature of the gas-sensing chamber was maintained at ~1.39% RH and RT (~27 ± 2 °C) respectively.

$$C(\text{ppm}) = C_{\text{std}}(\text{ppm}) \times f/f + F \quad (1)$$

Here f and F are the flow rate of target gas and the carrier gas, respectively.

The gas sensing properties were tested using picoammeter/voltage source (Keithely- 2400) connected to the hygrometer, temperature and mass flow controller and monitored using the PC installed with LabVIEW program. The surface of the sensor was illuminated with UV light ($\lambda = 365$ nm with a power density of 5.34 mW/cm^2) was installed on the quartz window of the test chamber.

2.3. Materials characterization

The crystalline structure of TiO_2 nanoplates were analyzed using the X-ray diffraction, HRXRD: Bruker D8 X-ray Diffractometer operating at 2.2 kW X-ray tube with Cu-Kα radiation ($\lambda = 1.54$ Å). The high-resolution transmission electron microscope (HR-TEM, HITACHI H-7650) and field-emission scanning electron microscopy (FESEM; Hitachi

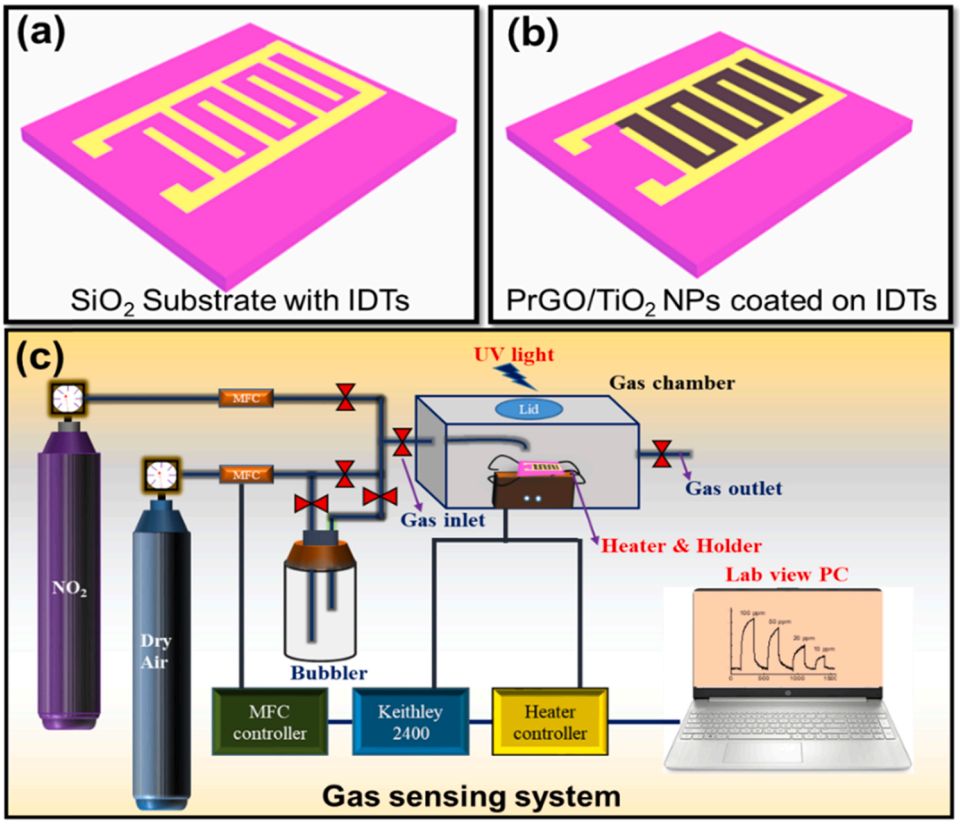

Fig. 1. Schematic illustration of the resistive gas sensor fabrication (a) the Interdigital electrode deposition on Si/SiO_2 substrate after organic cleaning, (b) Active material deposition on Interdigital electrodes of Si/SiO_2 substrate, (c) our gas sensing experimental gas sensor system setup.

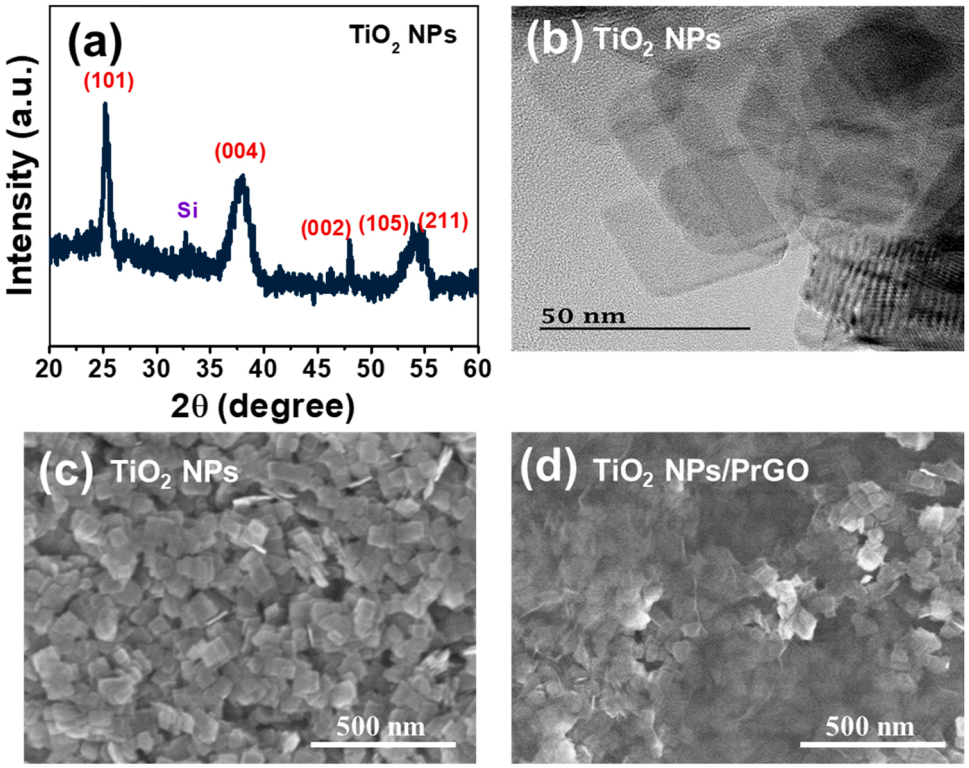

Fig. 2. (a) XRD peak of pristine TiO_2 nanoplates, (b) high resolution TEM image of TiO_2 NPs, SEM images of (c) pure TiO_2 NPs, and (d) TiO_2 NPs/PrGO hybrid nanocomposite.

S-4800) were employed to study the surface morphologies. Photoluminescence (Pl, LabRAM HR-800 and X-ray photoelectron spectroscopy (XPS; Thermo, VG Scientific Multilab 2000) analyses were performed to confirm the molecular hybridization between nanocomposites.

3. Results and discussions

X-ray diffraction (XRD) was conducted on TiO_2 NPs sample to identify the crystal facets. Fig. 2(a) depicts the patterns of TiO_2, which is good in agreement with the pure anatase-phase TiO_2 (JCPDS no. 21–1272) without any impurity phases. The peak positioned at $2\theta = 33^{\circ}$, corresponds to Si since the TiO_2 NPs was coated on it to measure the XRD spectra [10,18]. Fig. 2(b) shows HR-TEM image of TiO_2 NPs, and the inter-planar distance of the nanoplate was found to be ~0.235 nm, which was corresponding to the (001) facet of TiO_2 as presented in Fig. S1. These experimental results revealed that the TiO_2 NPs contained (001) planes which can be appears like an exposed flat surface [10,24]. Fig. 2(c and d) shows the FESEM images of pristine TiO_2 NPs and TiO_2 NPs/PrGO hybrid samples. It can be seen that both the samples were exhibited a nano plate like structure with a rectangular layout, which was in consistence with the TEM image. In addition, a wave like morphological structure appeared over the TiO_2 NPs represents the PrGO composite, which signifies the successful formation of hybrid nanocomposite heterostructure (Fig. 2(d)).

Further, XPS analyses were employed to gain the insight into the chemical composition and surface chemical states in the TiO_2 NPs/PrGO heterostructure. Fig. 3(a) displays the full surface survey spectra of TiO_2 NPs and TiO_2 NPs/PrGO hybrid sample was recorded in the range of 200–600 eV, which clearly indicating the major characteristic peaks of both the samples such as C 1 s, Ti, 2p and O 1 s. On the other hand, TiO_2 NPs/PrGO exhibited N 1 s peak around 400 eV additionally along with aforementioned peaks that clearly signifies the successful formation of the hybrid heterostructure. Fig. 3(b) show the Ti 2p spectrum composed with two dominant peaks positioned at 457.68 and 463.38 eV, which specifies the electronic states of Ti $2p_{3/2}$ and Ti $2p_{1/2}$ respectively. However, the Ti 2p peaks were shifted to 458.68 and 464.48 eV in TiO_2 NPs/PrGO heterostructure, which confirms the existence of charge transfer between PrGO nanocomposite and TiO_2 NPs [10,18]. Fig. 3(c) presents the C 1 s core-level spectra of TiO_2 NPs/PrGO, composed of three peaks at 284.78, 286.48 eV, and 288.58 eV were assigned to C-C, C-N, and C═O, respectively, which further confirms the successful incorporation of C and N atoms into the TiO_2 lattice [25]. The presence of these peaks revealed the existence of amines of PPD in rGO [26]. The N 1 s core-level peak of TiO_2 NPs/PrGO composite (Fig. 3(d)) containing amine- functional groups. Further resolution of N 1 s into three dominant peaks at 398.88, 399.68, and 402.78 eV, which are assigned to quinoid amine (−N =), benzoic amine (−NH^-), and cationic radical (N^+), respectively [22]. Next, Fig. 3(e) shows the O 1 s core level XPS spectra of TiO_2 NPs/PrGO, resolved into the three mains peaks positioned at 530.08, 530.98, and 531.98, which can be ascribed to the crystal lattice oxygen (O_C), deficient oxygen (O_V) and OH groups or adsorbed species (O_A), which would plays a vital role in the gas absorption [10,18]. Moreover, the photoluminescence (PL) analysis was conducted to explore the role of PrGO in charge separation at the TiO_2 NPs and PrGO heterointerface as shown in the Fig. 3(f). The PL studies were performed under 320 nm excitation wavelength at RT. It can be observed that the TiO_2 NPs exhibited two overlapped peaks at 395.8 and 469 nm and another emission peak at 528 nm. The emission peak at 395.8 nm is ascribed to the inter-band recombination, while the two peaks at 469 nm and 528 nm are due to the oxygen defects/vacancies in the TiO_2, which was attributed to the electron−hole recombination emission peak. Fascinatingly, the electron−hole recombination peak is decreased for both the TiO_2 NPs/PrGO and TiO_2 NPs/rGO than that of the pristine TiO_2 NPs that confirms the decreased recombination rate [18]. Thus, the incorporation of PrGO on the TiO_2 NPs surface signifies

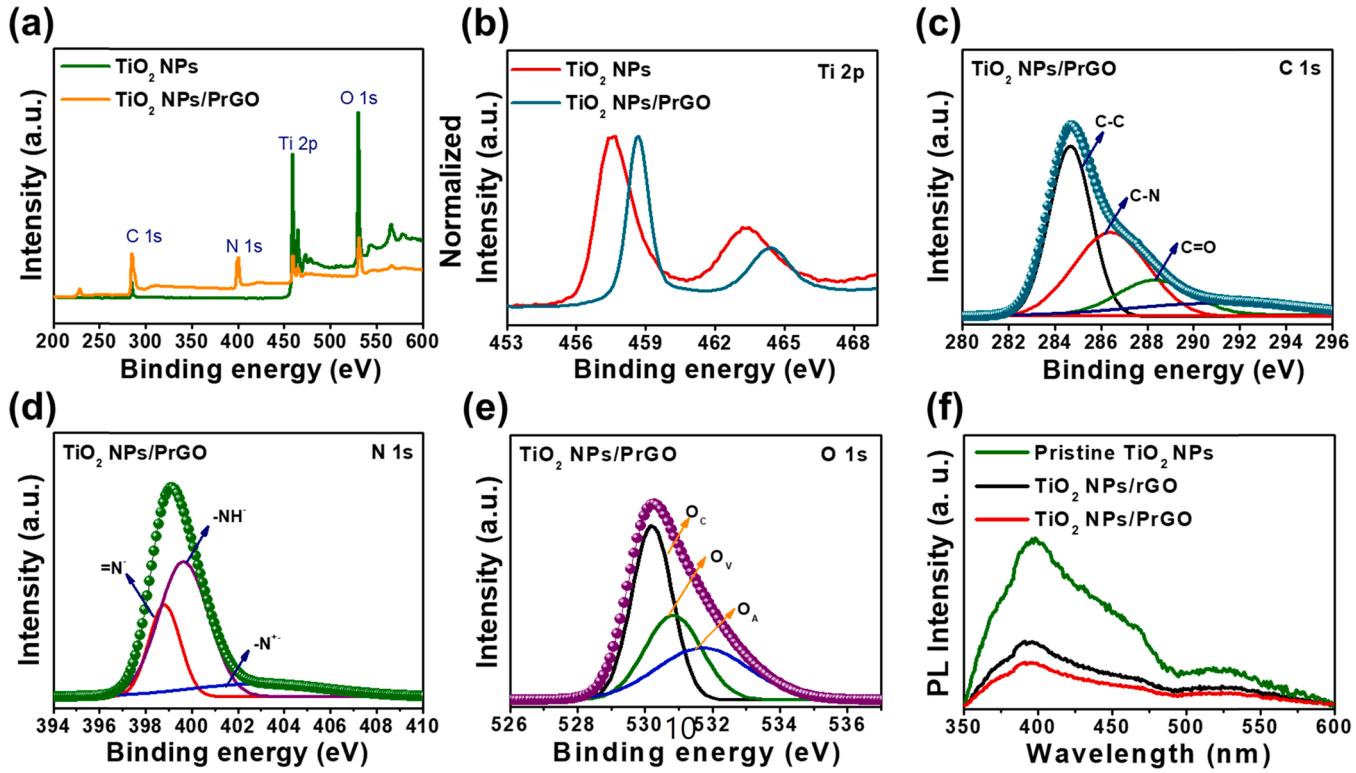

Fig. 3. (a) XPS full-survey scan spectra of pristine TiO_2 NPs and TiO_2 NPs/PrGO nanocomposite, XPS core level deconvoluted spectra of (b) Ti 2p, (c) C 1 s, (d) N 1 s, (e) O 1 s of TiO_2 NPs/PrGO nanocomposite, and (d) photoluminescence characteristics of TiO_2 NPs, TiO_2 NPs/rGO, and TiO_2 NPs/PrGO nanocomposites measured at RT.

the increase in separation efficiency of photogenerated charge carriers, which is favorable for the gas sensor applications. Hence, based on the fore mentioned analyses, the organic–inorganic hybrid network has given added advantage for more molecular/electronic interactions that can be tuned for more electro-active properties that effectively enhance the electron charge transfer in the TiO_2 NPs/PrGO heterostructure further helps to enhance the gas molecules absorption.

The effect of rGO, PrGO functionalization on the electrical properties of TiO_2 NPs was studied by I−V characteristics. Fig. 4(a) shows the current-voltage (I−V) characteristics of TiO_2 NPs/PrGO, TiO_2 NPs/rGO, and TiO_2 NPs at RT. It was seen that the pristine TiO_2 NPs shows the rectifying behavior since the Schottky barrier is existed at metal-TiO_2 NPs as similarly reported in the literature [27–29]. On the other hand, the TiO_2 NPs/ rGO composite exhibited improved rectifying behavior, which was raised from the hetero junction between TiO_2 NPs and rGO. However, it was noticed that the current levels of TiO_2 NPs/PrGO are high than that of rGO/TiO_2 NPs, which is possibly due to the high conductivity of PrGO [30]. We also investigated the I-V characteristics of TiO_2 NPs/PrGO in NO_2 ambient and it was noticed that the current levels were decreased in NO_2 ambient, which was attributed to the oxidation of TiO_2 NPs/PrGO at RT (Fig. 4(b)).

Fig. 5(a)-(c) shows the NO_2 gas sensing properties in terms of the samples resistance of pristine TiO_2 NPs, TiO_2 NPs/rGO, and TiO_2 NPs/PrGO by varying the different gas concentrations ranging from 10 to 100 ppm at RT. It was noted that the resistance of each device was escalated with increase in the gas concentration and reaches to a saturation level and then returned to its original base line resistance when NO_2 is turned off. It was to be noticed that TiO_2 NPs/PrGO exhibited high sensor resistance at each concentration compared to TiO_2 NPs/rGO and pristine TiO_2 NPs devices. The dynamic sensing responses were estimated using the following equation R_a-$R_g/R_a \times 100\%$, where R_a and R_g are the resistance at air and gas. The TiO_2 NPs/PrGO gas sensor yields a significant gas sensing response of about ~14.9% which was much higher than that of the pristine TiO_2 NP (~3.42%) TiO_2 NPs/rGO (~8.83%), and TiO_2 NPs/PPD (~5.42%, not shown here) to 100 ppm of NO_2 gas at RT, which was ascribed to synergetic effect of PPD and rGO composite matrix. The inset of Fig. 5(c) represented the stability test of TiO_2 NPs/PrGO, and the performance of the TiO_2 NPs/PrGO was quite stable and reproducible for the five repeated cycles. Moreover, the stable NO_2 gas sensing responses for the five consecutive repeatable cycles were estimated (Fig. S2(a)) and it showed a stable response of about ~14.9% to all the cycles without any distractions, which describes that the hybrid sensor has a good stability towards NO_2 gas (100 ppm) at RT. Furthermore, the long-term reproducibility (Fig S2(b)) of the hybrid sensor has been explored by testing the sensor for five consecutive weeks and the sensor showed a minute loss of ~1.05% in its total response to that of the starting day, further indicating the TiO_2 NPs/PrGO sensor has good reproducibility. These results clearly manifest that that the hybrid sensor exhibited enhanced sensitivity, stable response and significant reproducible characteristics to the NO_2 gas (100 ppm) at RT also as compared to the reported reports as presented in Table 1. Fig. 5(d) shows the distinguished relative response plots of the corresponding sensors measured at different gas analyte concentrations at RT, which was found as increased with an increase in gas NO_2 concentration. The linear fitting plots of the three sensors showed almost a linear response characteristics to the NO_2 gas analytes with a correlation coefficient of $R^2 = 0.943$, $R^2 = 0.957$ and $R^2 = 0.984$ respectively [3,10]. It can be observed that the gas sensor device with largest linear relationship, resulting to the more reliability in stable and reproducible gas sensing performances. To further, explore the TiO_2 NPs/PrGO device sensing performances, we have calculated the detection limit (DL) of the as prepared sensor using the following equation (Eqs. (2) and (3)) reported elsewhere [10].

$$DL(ppm) = 3\left(\frac{\mathrm{RMS_{noise}}}{\mathrm{Slope}}\right) \tag{2}$$

$$\mathrm{RMS_{noise}} = \sqrt{\left(R_i - R_f\right)^2 / \mathrm{N}} \tag{3}$$

Here, $\mathrm{RMS_{noise}}$ is the root mean square noise, which is the base-line noise level of the sensor response under air, estimated from the fifth-order polynomial fit as displayed in the Fig. S3(a). Where, R_i and R_f are the experimental data and the fitting points, extratced from the polynomial fit and N is the total number of base-line points. Whereas, the slope was retrived from the linear fitting of the response data points versus gas concentrations as shown in Fig. S3(b). Based on the above calculations we have estimated the theoretical DL of TiO_2 NPs/PrGO hybrid sensor of ~114 ppb, which was much the lowest value as compared to the other TiO_2 NPs/rGO (~204 ppb) and TiO_2 NPs (~435 ppb).

Furthermore, different strategies have been employed to enhance the gas sensor performance, and among those UV irradiations is one of the finest methods to enhance the device performance. Fig. 6(a) depicts the comparative response of TiO_2 NPs/PrGO under UV irradiation with a power density of 5.34 mW/cm^2 at RT to different ppm levels of NO_2 at RT. Fig. 6(b) and (c) show the response and recovery times of TiO_2 NPs/PrGO with and without UV illuminations. It was noticed that the UV light stimulates the response of the device compared to the darkness. The sensor displayed a response of 35.68% to 100 ppm of NO_2, which was more than doubled (2.35 times) the performance under darkness. Moreover, the response/recovery times of the TiO_2 NPs/PrGO sample was estimated using the exponential fitting [2] and it can be clearly seen that the response and recovery times of TiO_2 NPs/PrGO under UV light

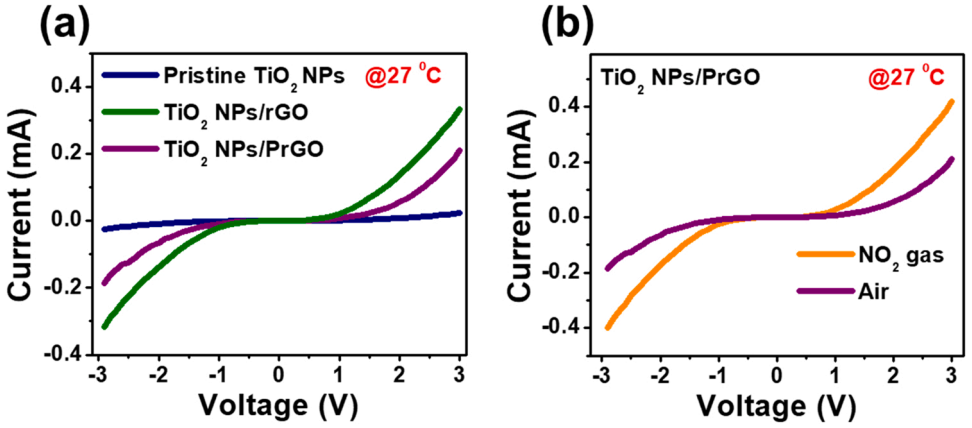

Fig. 4. (a) I-V characteristics of pristine TiO_2, TiO_2/rGO, and TiO_2/PrGO nanocomposites, (b) I-V characteristics of TiO_2 NPs/PrGO hybrid nancomposite under air and NO_2 gas ambient.

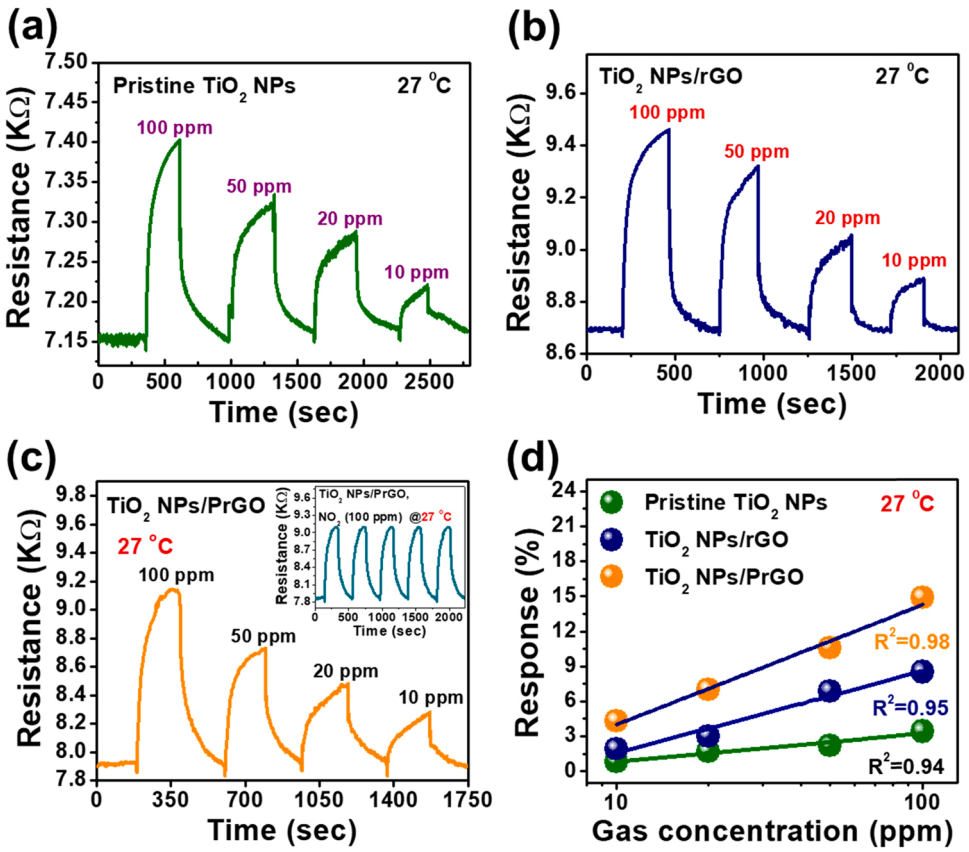

Fig. 5. The transient NO_2 gas (10–100 ppm) sensing response characteristic curves of (a) pristine TiO_2 NPs, (b) TiO_2 NPs/rGO, and (c) TiO_2 NPs/PrGO (inset image represents the cycling stability test) at RT, and (d) relative response of three different devices as a function of gas concentration at RT.

Table 1
Comparison of RT NO_2 gas sensing performances of our device with the previously reported literature.

Ref	Device structure	Target gas	Working-temperature (^{o} C)	Response (%)/ppm	Response/recovery time (sec)
[43]	RGO-CeO_2 hybrids	NO_2	RT	8.2/25	~180/260
[44]	In_2O_3–rGO	NO_2	RT	8.25/30	~165/235
[45]	TiO_2/ZnO	NO_2	200	7/5	~65/98
[46]	CuO-ZnO	NO_2	200	8/5	~13/60
[47]	Graphene/ZnO	NO_2	300	9.5/50	~145/248
[48]	ZnSe/ZnO	NO_2	200	10.42/10	~98/141
This work	TiO_2 NPs/rGO (dark)	NO_2	RT	14.9/100	~124/182
This work	TiO_2 NPs/rGO (UV)	NO_2	RT	35.6/100	~59/33

were much shorter (59 s and 33 s) than those in the dark condition (124 s and 182 s) to the 100 ppm of NO_2 as shown in Fig. 6(d). This was mainly ascribed to the low desorption rate of NO_2 from the surface of the sensor at dark conditions. Therefore, it is clear that the UV illumination effectively accelerated the response and recovery kinetics. This is reliable and reasonable since at higher gas concentration, a large number of gas molecules will be available to react at a given time, resulting in a short response time.

The effect of temperature on NO_2 gas sensing performance of TiO_2 NPs/PrGO at different temperature such as 27 °C (RT), 50 °C, 100 °C, and 150 °C were systematically studied by varying the NO_2 gas ppm concentrations (10–100 ppm) as shown in Fig. 7(a)–(b). It was noticed that the detection capability and sensitivity of TiO_2 NPs/PrGO was increased with increase in the temperature, which is possibly due to the high thermal energy that provides a large number of absorption sites, available at the interfaces between TiO_2 and PrGO, further leads to attract the large number of gas molecules at higher ppm concentrations [31]. Hence, the NO_2 gas sensing performance of TiO_2 NPs/PrGO sensor was fascinatingly enhanced at various temperature conditions, and the TiO_2 NPs/PrGO hybrid device exhibited the maximum response of 111.98% to 100 ppm of NO_2 at 150 °C, which was about ~8-fold times higher than that of the response obtained at RT.

Furthermore, the effect of relative humidity (RH) is another important factor that can effects the sensing performances of the practical gas sensor applications especially, operating at RT. Thus, effect of RH on the response characteristics of TiO_2 NPs/PrGO has been investigated at various RH conditions varying from 20% to 80% RH to the 100 ppm of NO_2 gas at RT as shown in the Fig. 8(a). It can be observed that response of the TiO_2 NPs/PrGO was drops considerably (~14.02–4.26%) when the RH levels escalates from 20% to 80%. The drastic fall in the sensing response of TiO_2 NPs/PrGO at higher RH levels (above 20% RH) was mainly due to the blocking of active surface sites by the water molecules on the heterostructure barrier, which could resist and minimizes the adsorption ability of O_2 molecules and further leads to difficult for the absorption of NO_2 gas molecules over the heterojunction surface [2,12]. In addition, selectivity is also another crucial factor for the real-time gas sensing applications. Therefore, selectivity test has been carried out for the sensor based on TiO_2 NPs/PrGO towards 100 ppm of NO_2, NO, HN_3,

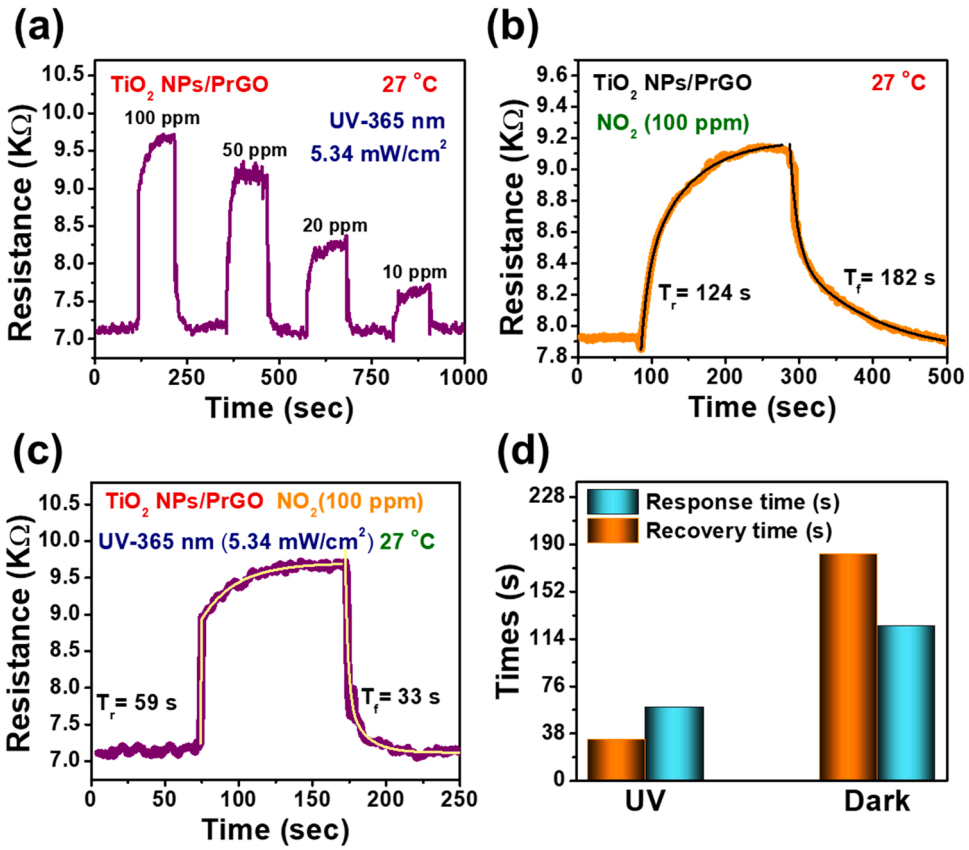

Fig. 6. NO_2 gas sensing properties of TiO_2 NPs/PrGO under UV illumination (365 nm with a power density of 5.34 mW/cm^2) at RT as a function gas concentration. Response and recovery times of TiO_2 NPs/PrGO (b) under darkness and (c) under UV illumination, and (d) relative summary comparison of response/recovery times of TiO_2 NPs/PrGO sensor under dark and UV conditions to the NO_2 (100 ppm).

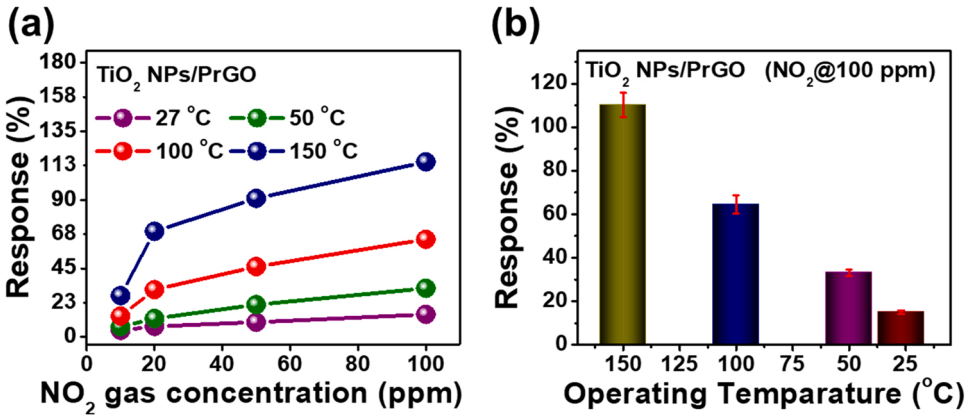

Fig. 7. (a) Temperature dependent dynamic NO_2 gas sensing properties of TiO_2 NPs/PrGO ranging from 27 °C to 150 °C, (b) relative response histograms of TiO_2 NPs/PrGO at different temperatures to 100 ppm at RT.

CO_2 and H_2 gas at RT as displayed in the Fig. 8(b). Obviously, the TiO_2 NPs/PrGO sensor showed significant and a very high gas sensing response towards the NO_2 gas among the other interferant gases, which clearly signifies that the sensor based on TiO_2 NPs/PrGO has an excellent capability to sense to NO_2 gas at RT.

The enhanced relative gas sensing responses of the TiO_2 NPs/PrGO hybrid heterostructure can be understood by using energy band diagram theory. Fig. 9(a and b) illustrates the gas sensing mechanism of the TiO_2 NPs/PrGO hybrid heterostructure using band theory under air and NO_2 gas ambient conditions. When the hybrid TiO_2 NPs/PrGO heterostructure was exposed to dry air at RT, the O_2 sites are created on the heterostructure since oxygen molecules were absorbed on active {001} facets of TiO_2, which was due to the presence of oxygen vacancies (written in Kröger-Vink notation ($V_O^{\bullet\bullet}$), given in Eqs. (4) and (5)) as discussed in XPS analysis. Next, the adsorbed oxygen species and gets ionized to form O_2, O^-, and O_2^- ionic species by withdrawing the electrons from heterostructure conduction band as given in Eqs. (6) and (7) [2,3,10,12]. These surface reactions would widen the depletion barrier at the TiO_2 NPs/PrGO heterostructure interface as the concentration of the free electrons decreased (Fig. 9(a)). When NO_2 gas is exposed upon heterostructure sensor surface, and the adsorbed NO_2 gas molecules change to NO_2^- [2,3,10,12]. Further, the NO_2^- species react

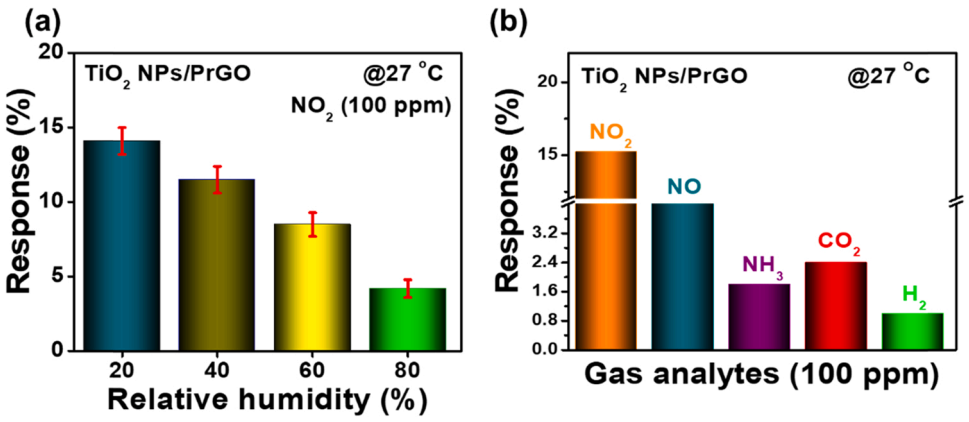

Fig. 8. (a) Response histograms of TiO_2 NPs/PrGO hybrid nanocomposite at various relative humidity condition ranging from 20% to 80% for 100 ppm of NO_2 gas at RT, (b) selectivity test histograms of TiO_2 NPs/PrGO towards various interferant gases NO_2, NO, HN_3, CO_2 and H_2 gas of 100 ppm at RT.

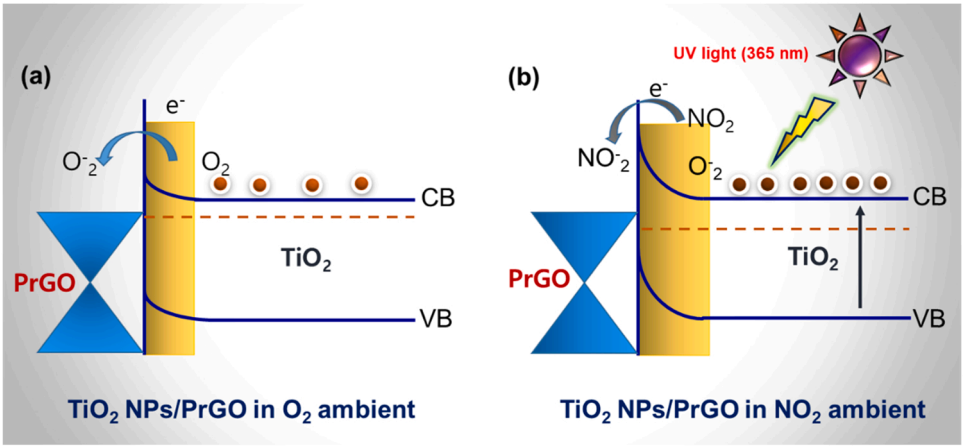

Fig. 9. Schematic illustration of the gas sensing mechanism of TiO_2 NPs/PrGO hybrid nanocomposite heterostructure under (a) air ambient and (b) NO_2 gas at RT.

with the surface-adsorbed O_2 species by withdrawing extra electrons from heterostructure, that further resulting into the decrease in electrons density (Eqs. 8–10). Thus, fermi level moves downwards that further causes to the increase in barrier height at the heterostructure interface as displayed in Fig. 9(b) [3,10,32,33].

$$O_O \leftrightarrow V_O^{\bullet\bullet} + 1/2\ O_2 + 2e^- \quad (4)$$

$$V_O^{\bullet\bullet}\ (gas) + O_2\ (gas) \rightarrow O_2\ (ads) + V_O^{\bullet\bullet} \quad (5)$$

$$O_2^-\ (ads) + e^- \rightarrow O_2^-\ (ads) \quad (6)$$

$$O_2^-\ (ads) + e^- \rightarrow O_2^{2-}\ (ads) + 2\ O^-\ (ads) \quad (7)$$

$$NO_2\ (gas) + e^- \rightarrow NO_2 + O_2 \quad (8)$$

$$NO_2\ (gas) + O_2^-\ (ads) \rightarrow NO_2^- + O_2 \quad (9)$$

$$2NO_2\ (gas) + O_2^-\ (ads) + e^- \rightarrow 2NO_3^- \quad (10)$$

Moreover, the high gas sensing response of the TiO_2 NPs/PrGO heterostructure was mainly ascribed to the oxygen vacancies, OH and amine functional groups that helps to improve the adsorption and desorption kinetics of gaseous molecules at the heterojunction interface, which further results in the change in resistance of the hybrid TiO_2 NPs/PrGO sensor under NO_2 gas [10,32–34]. In addition, the NO_2 gas molecules would absorb on the surface through the physisorption and chemisorption process. In these two processes, the absorbed gas molecules needs high energy to desorb, which was due to the existence of the strong hybridization between the heterostructure [35,36]. Hence, in the present study we used the UV light illumination effect to further improve the gas sensing properties through the fast desorption rate.

The TiO_2 NPs/PrGO hybrid heterostructure would effectively separate the photo-generated charge carriers due to the existence of heterojunction between TiO_2 NPs and PrGO nanocomposite as shown in Fig. 9 (b). The high absorption and the high quantum efficiency of the PPD promotes the generation of high photocurrent upon the illumination [37,38]. The molecular functionalization between PPD and rGO provides a high conductive channel through the PrGO nanocomposite matrix, which acts as electron transport layer. Under UV light illumination, large number of electron hole (*e-h*) pairs were generated and which may get effectively separated due to the existence of high built-in potential at the junction interface [2,12,18]. Then the absorbed O_2 molecules seize the electrons, which are generated under UV illumination and enlarge the oxygen ionization rate (Eqs. 11–13). In which, the generated holes could effectively help to improve the desorption rate as given in Eq. (13). In addition, the molecular sensitivity of PrGO nanocomposite to NO_2 gas would be high due to the existence of amine-rich PPD and the enhanced OH and amine functional groups [38]. The NO_2 gas molecules withdraw the electrons from TiO_2 NPs/PrGO hybrid nanocomposite conduction band due to its high electronegativity. This further widens the TiO_2 NPs/PrGO depletion layer leading to the resistance increase in the sensor under NO_2 gas ambient. Moreover, under the UV light excitation the photo-induced e-h pairs were fascinatingly separated at the heterointerface junction due to the low recombination probability raised by the synergetic effect of the hybrid heterostructure, which was supported by the PL analysis. Hence, the generated *e-h* pairs under UV light could

be attributed to the enhancement in the NO_2 gas absorption and promotes the excellent charge transfer between the gas analytes and the hybrid nanocomposite surface that further, results in the high gas sensing response and fast response/recovery times as compared to the dark condition [39–42].

$$h\nu \rightarrow h^+ + e^- \quad (11)$$

$$O_2 + e^- (h\nu) + O_2^-(h\nu) \quad (12)$$

$$O_2^-(ads) + h^+(h\nu) \rightarrow O_2\,(gas) \quad (13)$$

Where $h\nu$ is the incident photonic energy, h^+, e^- are the generated holes and electrons inside the semiconductor, *ads* represents the adsorption and O_2^- is the chemisorbed oxygen ion. Henceforth, the outstanding response of the device in various environmental conditions like dark, UV illumination and different humidity conditions signifies that our sensor on PrGO-decorated TiO_2 NPs is a suitable candidate for RT NO_2 gas sensor applications.

4. Conclusion

In summary, the TiO_2 NPs/PrGO hybrid heterostructure was successfully fabricated and tested for the effective detection of NO_2 gas at RT. A series of SEM, XPS and PL analyses were confirmed the formation of the hybrid nanocomposite and efficient charge transfer in between the hybrid nanocomposite. The functionalization of PrGO on TiO_2 nanoplates stimulated the NO_2 absorption by the combined effect of oxygenous and amines functional groups on the PrGO surface. The TiO_2 NPs/PrGO exhibited a significant gas response (~14.9%) which was 4.57 fold times high, with an excellent selectivity, high sensitivity fast response/recovery and repeatability towards NO_2 (100 ppm) at RT as compared to pristine counter parts. Further, the NO_2 gas sensing performances of the TiO_2 NPs/PrGO sensor was boosted by the irradiation of UV light and the gas detection response (35.68%) was found to be increased 2.35 fold times with short response/recovery times (59 s/33 s) than that of the responses measured at under dark condition. Furthermore, the hybrid sensor was tested under various RH conditions and the test results revealed that the sensing responses of the device was decreased with enhancement in RH values, however, the performances of the device were found to be stable. Moreover, the sensing mechanism has been proposed based on the efficient charge carrier generation, separation, and prevention of recombination due to the heterointerface junction formation between the hybrid nanocomposites. Thus, we anticipate that our hybrid composites can be considered as promising sensing materials for practical application of NO_2 detection at RT.

CRediT authorship contribution statement

Nimmala Harathi: Conceptualization, Experiments, Data curation, Writing - original draft. **Manoj Bollu:** Conceptualization, Experiments, Data curation, Writing - original draft. **Kedhareswara Sairam Pasupuleti:** Investigation, Visualization, Data curation, Writing review & editing. **Zhandos Tauanov:** Formal analysis. **Koteswara Rao Peta:** Formal analysis. **Moon-Deock Kim:** Formal analysis, Resources. **Maddaka Reddeppa:** Conceptualization, Visualization, Methodology, Investigation, Data curation, Validation, Writing - original draft. **Argha Sarkar:** Visualization, Validation, Investigation, Review & editing. **Vempuluru Navakoteswara Rao:** Supervision, Resources, Methodology, Visualization, Validation, Investigation, Writing - review & editing.

Declaration of Competing Interest

The authors declare that they have no known competing financial interests or personal relationships that could have appeared to influence the work reported in this paper.

Acknowledgement

Authors would like sincerely thank Dr. G. Murali, for providing TEM analysis, Dr. M. Reddeppa for his valuable guidance and constructive suggestion, Dr. Singiri Ramu for his motivation for this work. We also thanks to Prof P.K Rao & Prof M.D Kim for their kind support.

Appendix A. Supporting information

Supplementary data associated with this article can be found in the online version at doi:10.1016/j.snb.2022.131503.

References

[1] Md.A. Hossain Khan, et al., Reliable anatase-titania nanoclusters functionalized GaN sensor devices for UV assisted NO_2 gas-sensing in ppb level, Nanotechnology 31 (2020), 155504.
[2] M. Reddeppa, et al., Interaction activated interfacial charge transfer in 2D g-C_3N_4/GaN nanorods heterostructure for self-powered UV photodetector and room temperature NO2 gas sensor at ppb level, Sens. Actuators B Chem. 329 (2021), 129175.
[3] J. Jaiswal, et al., Low-temperature highly selective and sensitive NO2 gas sensors using CdTe-functionalized ZnO filled porous Si hybrid hierarchical nanostructured thin films, Sens. Actuators B Chem. 327 (2021) (2021). Article 128862.
[4] S. Thirumalairajan, et al., Surface morphology-dependent room-temperature lafeo3 nanostructure thin films as selective NO2 gas sensor prepared by radio frequency magnetron sputtering, ACS Appl. Mater. Interfaces 6 (2014) 13917–13927.
[5] R. Kumar, et al., Two-Dimensional, Few-Layer $MnPS_3$ for Selective NO_2 Gas Sensing under Ambient Conditions, ACS Sens 5 (2020) 404–411.
[6] J.W. Kim, et al., Micropatternable double-faced ZnO nanoflowers for flexible gas sensor, ACS Appl. Mater. Interfaces 9 (2017) 32876–32886.
[7] Y. Lin, et al., Fully gravure-printed NO_2 gas sensor on a polyimide foil using WO_3-PEDOT:PSS nanocomposites and Ag electrodes, Sens. Actuators B Chem. 216 (2015) 176–183.
[8] M. Li, et al., Radiation enhancement by graphene oxide on microelectromechanical system emitters for highly selective gas sensing, ACS Sens 4 (2019) 2746–2753.
[9] rao Navkoteswar, et al., Manifestation of enhanced and durable photocatalytic H2 production using hierarchically structured Pt@Co3O4/TiO2 ternary nanocomposite, Ceram. Int. 47 (2021) (2021) 10226–10235.
[10] Kedhareswara Sairam Pasupuleti, et al., High performance langasite based SAW NO2 gas sensor using 2D g-C3N4@ TiO2 hybrid nanocomposite, J. Hazard. Mater. 427 (2021) (2022), 128174.
[11] W. Geng, et al., Morphology-dependent gas sensing properties of cuo microstructures self-assembled from nanorods, Sens. Actuators B 325 (2020), 128775.
[12] Reddeppa, et al., NOx gas sensors based on layer-transferred n-MoS_2/p-GaN heterojunction at room temperature: Study of UV light illuminations and humidity, Sens. Actuators B 308 (2020), 127700.
[13] D. Panda, et al., Selective detection of carbon monoxide (CO) gas by reduced graphene oxide (rGO) at room temperature, RSC Adv. 6 (2016) 47337–47348.
[14] M.W. Jung, et al., Highly transparent and flexible NO_2 gas sensor film based on MoS_2/rGO composites using soft lithographic patterning, Appl. Suf. Sci. 456 (2018) 7–12.
[15] V.S. Bhati, et al., NO_2 gas sensing performance enhancement based on reduced graphene oxide decorated V_2O_5 thin films, Nanotechnology 30 (2019), 224001.
[16] M. Chen, et al., Porous ZnO Polygonal Nanoflakes: Synthesis, Use in High-Sensitivity NO_2 Gas Sensor, and Proposed Mechanism of Gas Sensing, J. Phys. Chem. C. 115 (2011) 12763–12773.
[17] J. Wu, et al., Three-Dimensional Graphene Hydrogel Decorated with SnO_2 for High-Performance NO2 Sensing with Enhanced Immunity to Humidity, ACS Appl. Mater. Interfaces 12 (2020) 2634–2643.
[18] G. Murali, et al., Enhancing the charge carrier separation and transport via nitrogen-doped graphene quantum dot-TiO_2 nanoplate hybrid structure for an efficient NO gas sensor, ACS Appl. Mater. Interfaces 12 (11) (2020) 13428–13436.
[19] Hao, et al., Controllable synthesis and enhanced gas sensing properties of a single-crystalline WO3–rGO porous nanocomposite, RSC Adv. 7 (2017) 14192–14199.
[20] Reddeppa, et al., UV-light enhanced CO gas sensors based on InGaN nanorods decorated with *p*-Phenylenediamine-graphene oxide composite, Sens. Actuator B Chem. 307 (2020), 127649.
[21] D. Li, et al., One-pot synthesis and electrochemical properties of graphene/SnO2/poly (p-phenylenediamine) ternary nanocomposites, J. Alloy. Compd. 652 (2015) 9–17.
[22] N.D. Chinh, et al., UV-light-activated H_2S gas sensing by a TiO_2 nanoparticulate thin film at room temperature, J. Alloy. Compd. 778 (2019) 247–255.
[23] T. Chandrakalavathi, et al., p-Phenylenediamine functionalized rGO/Si heterostructure Schottky junction for UV photodetectors, Diam. Relat. Mater. 93 (2019) 208–215.
[24] Y. Yang, et al., Efficient Charge Separation from F−Selective Etching and Doping of Anatase-TiO_2{001} for Enhanced Photocatalytic Hydrogen Production, ACS Appl. Mater. Interfaces 10 (2018) 19633–19638.

[25] Song, et al., Molecular level study of graphene networks functionalized with phenylenediamine monomers for supercapacitor electrodes, Chem. Mater. 28 (2016) 9110.
[26] K. Zhang, Graphene/polyaniline nanofiber composites as supercapacitor electrodes, Chem. Mater. 22 (2010) 1392–1401.
[27] Deb Prasenjit, Low Dark Current and High Responsivity UV Detector Based on TiO2 Nanowire/RGO Thin Film Heterostructure, IEEE Trans. Electron Devices 66 (2021) 3874–3880.
[28] Minh Triet Nguyen, et al., High-Performance Schottky Diode Gas Sensor Based on the Heterojunction of Three-Dimensional Nanohybrids of Reduced Graphene Oxide−Vertical ZnO Nanorods on an AlGaN/GaN Layer, ACS Appl. Mater. Interfaces 9 (2017) 30722–30732.
[29] P. Cao, et al., Down to ppb level NO_2 detection by ZnO/rGO heterojunction based chemiresistive sensors, Chem. Eng. J. 401 (2020), 125491.
[30] B. Ramezanzadeh, et al., Effects of highly crystalline and conductive polyaniline/graphene oxide composites on the corrosion protection performance of a zinc-rich epoxy coating, Chem. Eng. J. 320 (2017) 363–375.
[31] Geetanjali Deokar, MoS_2–Carbon Nanotube Hybrid Material Growth and Gas Sensing, Adv. Mater. Interfaces 4 (2017), 1700801.
[32] Vishnuraj Ramakrishnan, Porous, n–p type ultra-long, ZnO@Bi2O3 heterojunction nanorods - based NO2 gas sensor: new insights towards charge transport characteristics, Phys. Chem. Chem. Phys. 22 (2020) 7524–7536.
[33] Siowwoon Ng Atomic Layer Deposition of SnO_2-Coated Anodic One-Dimensional TiO2 Nanotube Layers for Low Concentration NO_2 Sensing, *ACS Appl. Mater. Interfaces* 2020, 12, 29, 33386–33396.
[34] Nagmani, et al., Highly sensitive and selective H2S gas sensor based on TiO2 thin films, Appl. Sur. Sci. 549 (2021), 149281.
[35] Di Liu, Visible light assisted room-temperature NO_2 gas sensor based on hollow SnO_2@SnS_2 nanostructures, Sens. Actuator B Chem. 324 (2020), 128754.
[36] Yi Xia, Highly Sensitive and Fast Optoelectronic Room-Temperature NO_2 Gas Sensor Based on ZnO Nanorod-Assembled Macro-/Mesoporous Film, ACS Appl. Electron. Mater. 2 (2) (2020) 580–589.
[37] Wu Tong, et al., UV excitation NO_2 gas sensor sensitized by ZnO quantum dots at room temperature, Sens. Actuator B Chem. 259 (2018) 526–531.
[38] A. Wang, Reduced graphene oxide covalently functionalized with polyaniline for efficient optical nonlinearities at 532 and 1064 nm, Dyes Pigments 160 (2019) 344–352.
[39] Su Yuanjie, et al., Self-powered room temperature NO_2 detection driven by triboelectric nanogenerator under UV illumination, Nano Energy 47 (2018) 316–324.
[40] Sunghoon Park, Synthesis, structure, and UV-enhanced gas sensing properties of Au-functionalized ZnS nanowires, Sens. Actuator B: Chem. 188 (2013) 1270.
[41] S. Park, UV-Enhanced NO_2 Gas Sensing Properties of SnO_2-Core/ZnO-Shell Nanowires at Room Temperature, ACS Appl. Mater. Interfaces 10 (2013) 4285–4292, 2013, 5.
[42] Ehsan Espid, et al., Development of highly sensitive ZnO/In_2O_3 composite gas sensor activated by UV-LED, Sen. Actuators B Chem. 241 (2017) 828.
[43] Ji Hu et al. 2018 Light-assisted recovery for a highly-sensitive NO_2 sensor based on RGO-CeO_2 hybrids.
[44] F. Gu et al. 2015 In_2O_3–graphene nanocomposite based gas sensor for selective detection of NO_2 at room temperature.
[45] N. Ramgir, et al., TiO2/ZnO heterostructure nanowire based NO_2 sensor, Mater. Sci. Semicond. Process. 106 (2020) (2020), 104770.
[46] S.M. Mali, et al., Heterostructural CuO-ZnO nanocomposites: a highly selective chemical and electrochemical NO2 sensor, ACS Omega 4 (2019) (2019) 20129–20141.
[47] H.W. Kim, et al., Synthesis of zinc oxide semiconductors-graphene nanocomposites by microwave irradiation for application to gas sensors, Sens. Actuators B Chem. 249 (2017) (2017) 590–601.
[48] W. Liu, et al., Ultrasensitive NO_2 detection utilizing mesoporous ZnSe/ZnO heterojunction-based chemiresistive-type sensors, ACS Appl. Mater. Interfaces 11 (2019) 29029–29040.

Nimmala Harathi received her M. Tech degree from JNTU Hyderabad and she is currently working as an assistant professor at Electronics & Instrumentation Engineering, Sree Vidyanikethan Engineering College, Tirupati 517102, India. Her research interest are developing actuators, MEMS and SAW based sensors, nano materials, COMSOL simulation.

Manoj Bollu received his Master's degree in Physics with a specialization of thin films and vacuum technology from Sri Venkateswara University, Tirupati, India, in 2019. His current research interests includes synthesis of nanomaterials and thin films using RF sputtering for gas sensing and optoelectronic applications.

Kedhareswara Sairam Pasupuleti received his Master's degree in Physics with a specialization of Thin films and Vacuum technology from Sri Venkateswara University, Tirupati, India, in 2018. He is a Ph.D. student in the department of Physics, Chungnam National University, Republic of Korea. His current research interests include fabrication of SAW based gas sensors and III-nitride semiconductor materials for optoelectronics and gas sensor applications.

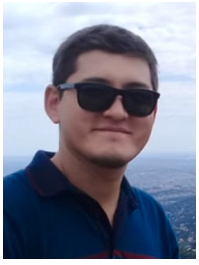

Dr. Zhandos Tauanov he is currently working as Assistant Professor at al-Farabi Kazakh National University, Faculty of Chemistry and Chemical Technology, Almaty, Kazakhstan, 050040.

Dr. Koteswara Rao Peta received B. Sc (2003) and M. Sc (2005) degrees in Physics from the Sri Venkateswara University. He awarded Ph.D degree in Electronics from the University of Mysore in 2010. He worked as post-doctoral researcher at the department of Physics, Chungnam National University, South Korea. Since 2013, he has been an assistant professor in the Electronic Science at University of Delhi, India. His current research include wide band gap semiconductors, gas sensors and optoelectronic devices.

Prof. Moon-Deock Kim received his Ph.D in department of semiconductor physics at Dongguk University, Republic of Korea in 1994. Currently he is professor of physics department at Chungnam Nat. Univ., Republic of Korea. His current research interests are Gas sensors, Photodetectors and III–V nitride semiconductor growth and device processing including LED'S, Solar cell, Surface acoustic wave sensors and High Electron mobility transistors.

Dr. Maddaka Reddeppa received his PhD in Physics, Chungnam Nat. Univ., Republic of Korea in August 2019. He is currently working as a post-doctoral researcher at University of Michigan, Ann Arbor USA. His current research interests include synthesis and characterization of III-nitride semiconductor materials for optoelectronics and gas sensor applications.

Dr. Argha Sarkar is a Visvesvaraya Fellow, MeitY, Govt. of India, and currently working as an Associate Professor in the dept. of Electronics & Communication Engineering, Vishnu Institute of Technology (A), Andhra Pradesh, India. he has received his M. Tech and doctoral degree from NIT Arunachal Pradesh. He has authored several book chapters, published research papers in reputed international journals, conferences and associated with many professional bodies like IEEE, IE, ISTE etc. M. Tech and PhD research scholars are presently working under him. He is instrumental in setting up fabrication lab and proficient in device fabrication. His research interest are developing metal oxide based gas sensor, MEMS and SAW based transducers and biosensors.

Dr. V. Navakoteswara Rao received his Ph.D. degree from the Department of Materials Science & Nanotechnology, Yogi Vemana University, Kadapa, Andhra Pradesh, 516005 India. He is currently working as a Senior Scientist under the Brain Pool program in the national nanofabrication center at Korea Advanced Institute of Science and Technology, Republic of Korea. His research interests in designing and developing nanomaterials as photocatalysts for energy applications, and the major synthesis and characterizations of 3d metal oxide/metal chalcogenides, metal nitrides, metal phosphides, perovskites, and metal carbides for augmented photocatalytic properties, water splitting, energy applications, and gas sensors.